Mining Science, vol. 26, 2019, 91–108

www.miningscience.pwr.edu.pl

Mining Science

(Previously Prace Naukowe Instytutu Gornictwa Politechniki Wroclawskiej, ISSN 0370-0798)

ISSN 2300-9586 (print)
ISSN 2353-5423 (online)

Received January 27, 2018; reviewed; accepted May 24, 2019

LABORATORY TESTS ON E-PELLETS EFFECTIVENESS FOR ORE TRACKING

Mo-Ewn XIE[1], Fu-Xia LV[1]*
Li-Wei WANG[2]

[1] School of Civil and Resource Engineering, University of Science and Technology Beijing, Beijing 100083, China
[2] College of Civil Engineering and Mechanics, Yanshan University, Qinhuangdao 066004, China

Abstract: Landslides generally cause more damage than first predicted. Currently, many methods are available for monitoring landslides occurrence. Conventional methods are mainly based on single-point monitoring, which omits the aspect of variation in large-scale landslides. Due to the development of radar satellites, the differential interferometric synthetic aperture radar technique has been widely used for landslide monitoring. In this study, an experimental region in the Wudongde Hydropower Station reservoir area was studied using archived spaceborne synthetic aperture radar (SAR) data collected over many years. As the permanent scatterer interferometric SAR (PS-InSAR) technique is an advanced technology, it could be suitably used to overcome the time discontinuity in long time series. However, the accuracy of date processing obtained using the PS-InSAR technique is lower than that obtained using the single-point monitoring method. The monitoring results of the PS-InSAR technique only demonstrate the moving trend of landslides and do not present the actual displacement. The Advanced Land Observation Satellite and a high-precision total station were used for long-term landslide monitoring of the Jinpingzi landslide at the Wudongde Hydropower Station reservoir area. Based on a relationship analysis between the data obtained using the PS-InSAR technique and the total station, a revised method was proposed to reduce the errors in the PS-InSAR monitoring results. The method can not only enhance the monitoring precision of the PS-InSAR technology but also achieve long-term monitoring of landslide displacement from a bird's-eye view.

Keywords: *landslide monitoring, PS-InSAR technology, reservoir landslide, error analysis*

* Corresponding authors: b20140024@xs.ustb.edu.cn (F. Lv)

doi: 10.5277/msc192607

1. INTRODUCTION

A common natural disaster, landslides not only cause damage to infrastructure but also results in casualties. It is worthwhile to research how and when this natural disaster occurs. Based on the current findings, a landslide usually occurs due to long-term stress accumulation and dynamic processes. A landslide comprises peristaltic, sliding, and violent sliding stages (Kong et al. 2004). Xu et al. stated that the landslide formation stage comprises the peristaltic deformation, rapid deformation, sliding, and gradual stabilization stages (Xu et al. 2012). Thus, it is important to conduct a long-term observation of landsides and determine their accumulative deformation. Remote monitoring can be used to study the minor and continuous changes that occur at the landslide slide. An advantage of remote monitoring is that it enables the early detection of a landslide. This can considerably reduce losses during a landslide in terms of the damage caused to infrastructure human lives. Applied landslide monitoring methods vary depending on the landslide development conditions. A landslide that slips slowly with an annual movement rate of less than 160 m in the early stage of formation (Cruden et al. 1996) is termed a slow-moving landslide and can be continuously monitored using remote sensing (RS) technology over a large area (Wang et al. 2013).

RS can provide a range of data covering hundreds to thousands of square kilometers without requiring personnel intervention and is considerably advantageous for conducting landslide monitoring over a large natural mountain area (Wang et al. 2011). When the differential interferometric synthetic aperture radar (D-InSAR) technique is used to detect a tiny deformation on the land surface, a detection ability in centimeters or even on a even smaller scale is obtained, thus making the D-InSAR technique suitable for landslide monitoring. For example, Catani used ERS-1/2(Earth Resources Satellite) to monitor landslides in Valdarno Superio and Laion in Italy (Catani et al., 2005). Singhroy used RADARSAT-1 data to monitor the Canadian Thunder River landslide (Singhroy et al. 2008). Xie used RADARSAT-2 data to identify a landslide in the Wudongde Reservoir region of China (Xie et al., 2016). However, the loss of coherency limits the application of D-InSAR technology for in landslide monitoring. Based on imaging observation stability in the target object tracking area and by monitoring the permanent scatterer (PS) in the changing process of a long time series, a reliable method for obtaining deformation monitoring results was developed, namely the use of a permanent scatterer interferometric synthetic aperture radar (PS-InSAR) (Ferretti et al. 2000; 2001).

With high precision, PS-InSAR technology can process long time series images and is widely used in the deformation monitoring of slow-moving landslides. Hastaoglu processed PS and GNSS data together and obtained movement models for the line of slight (LOS) velocities. These models were applied for the monitoring of slow-moving landslides in Koyulhisar (Hastaoglu et al. 2016). Bovenga combined the surface deformation information detected using the PS-InSAR technology with geological geomorphology data for monitoring the slow-moving landslides in the mountains of southern

Italy (Bovenga et al. 2006). Bianchini detected potential peristaltic landslides by conducting spatial analysis and clustering of surface deformation information obtained using PS-InSAR technology (Bianchini et al. 2012; 2013). Lu collected the synthetic aperture radar (SAR) data of 102 scenes from the RADARSAT-1 satellite and used the PS-InSAR technique to conduct quantitative disaster assessment of a slow-moving landslide that was spread across 9130 km2 in the Arno River basin, Italy (Lu et al. 2014). Calvello combined statistics with the PS-InSAR technique to qualitatively analyze a slow-moving landslide spread across 490 km2 in southern Italy (Calvello et al. 2016). By using the PS-InSAR technique, Lei successfully located the landslide area at Berkeley Hills and obtained the deformation rate of the terrain (Lei et al. 2012). As aforementioned, previous studies have successfully used PS-InSAR technology for monitoring slow-moving landslides and have provided a many valuable results. However, due to inevitable errors in data acquisition when SAR technology is used, the accuracy of single-point monitoring is not as high as that of traditional technology, such as global positioning system or total station monitoring. By analyzing the long time series obtained using the PS-InSAR technique and the relationship between the monitoring data obtained using total station monitoring and the PS-InSAR technique, the authors developed and presented a PS-InSAR error correction method in this study based on the landslide monitoring results in the surface domain obtained using PS-InSAR technology in Southwest China.

2. PS-INSAR TECHNOLOGY PROCESS

PS-InSAR can use multiple images to generate several interferences in a time series. Then, these interferences can be subjected to differential processing. This helps to sepa-

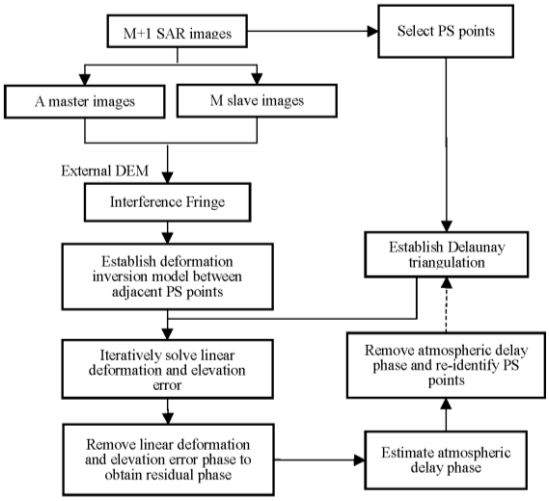

Fig. 1. PS-InSAR Technical flow chart

rate topographic phase information from multiple interference relatives. Finally, the surface deformation information can be extracted. A schematic map of the PS-InSAR process is displayed in Fig. 1.

3. STUDY AREA AND DATA

3.1. THE STUDY AREA

The study area is located at the Jinsha River basin in Southwest China, and the Jinpingzi landslide is located near Wudongde Hydropower Station. The landslide had a spindle-like shape in the plane and was distributed along the east–west direction. The length of the landslide was approximately 3 km, the width of the leading edge was approximately 1.5 km, and the width of the trailing edge was approximately 1.2 km. The leading edge and the trailing edge had an arc shape, and the elevation difference between them was approximately 1100 m. The Jinpingzi landslide occurred close to the site of Wudongde Dam. Thus, the stability of the landslide directly affected the construction and safety of Wudongde Hydropower Station. The location and surrounding environment of the Jinpingzi landslide are displayed in Fig. 2.

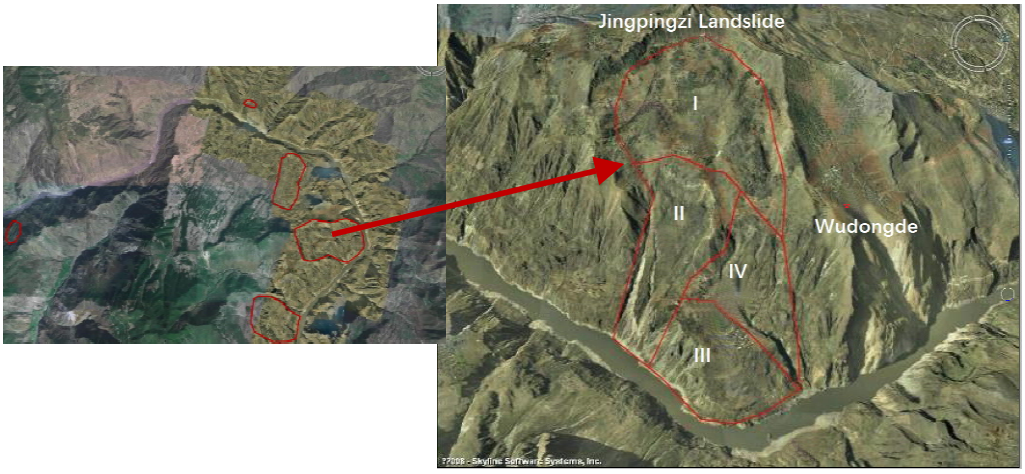

Fig. 2. Study area location map

3.2. THE DATA TYPE

This study uses ten-sence three frames up-track SAR data, which are obtained by the ALOS satellite PALSAR sensor. The images acquisition took place from 2007 to 2009.

All images are taken in the up-track shooting mode. The coverage of each image is 20×20 km^2. Horizontal polarization (HH) and the L band were used, and the spatial resolution was 6.25 m. The specific parameters are presented in Table 1.

Table 1. ALOS PALSAR Data parameter table

Date	Shooting mode	Polarization mode	Incident angle	Band	Coverage area	Time period
2007/1/18 2007/7/12 2007/10/12 2008/1/12 2008/2/27 2008/4/13 2008/7/14 2008/11/29 2009/3/1 2009/9/1	Ascending	HH	38.7°	L-band	20 km × 20 km	46 d

PS-InSAR processing generated nine interference relatives from ten SAR images. In consideration of the influence of the spatial-temporal baseline distance and the Doppler centroid frequency baseline on the decoherence of the interference images, the images from July 12, 2007 was selected as the common master image to perform differential interference processing with other images. After PS-InSAR baseline link processing was conducted, the relationships between the time baseline and the space baseline for each image and the common master image were obtained. The results are presented in Fig. 3.

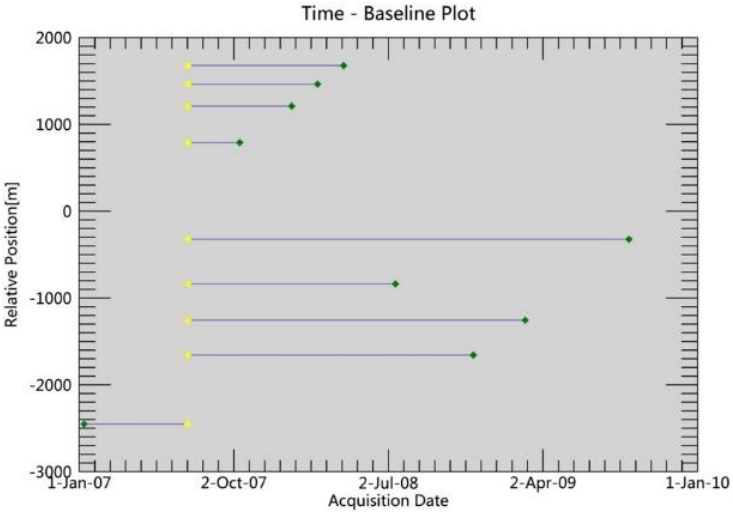

Fig. 3. The relationship of time baseline and space baseline

between each image and the master image

3.3. PS POINT SELECTION

Through phase filtering, phase unwrapping, the flattening effect, and the registration of the common master image and the remaining nine slave images, the master image was resampled into the common master image space to obtain an interferogram. Then, nine differential interferograms were obtained by conducting differential interference processing. Subsequently, the candidate points of PS and the rate estimate were obtained by performing a back-calculation for the first time. Then, a second back-calculation was conducted to remove the atmospheric phase and re-estimate the displacement and velocity. Finally, the average rate map and displacement map of each time series were generated through geocoding. Moreover, displacement and velocity vector diagrams were generated using the displacement values and rate values at each PS point. The distribution density was 39 PS points/km^2. The distribution of PS points is displayed in Fig. 4.

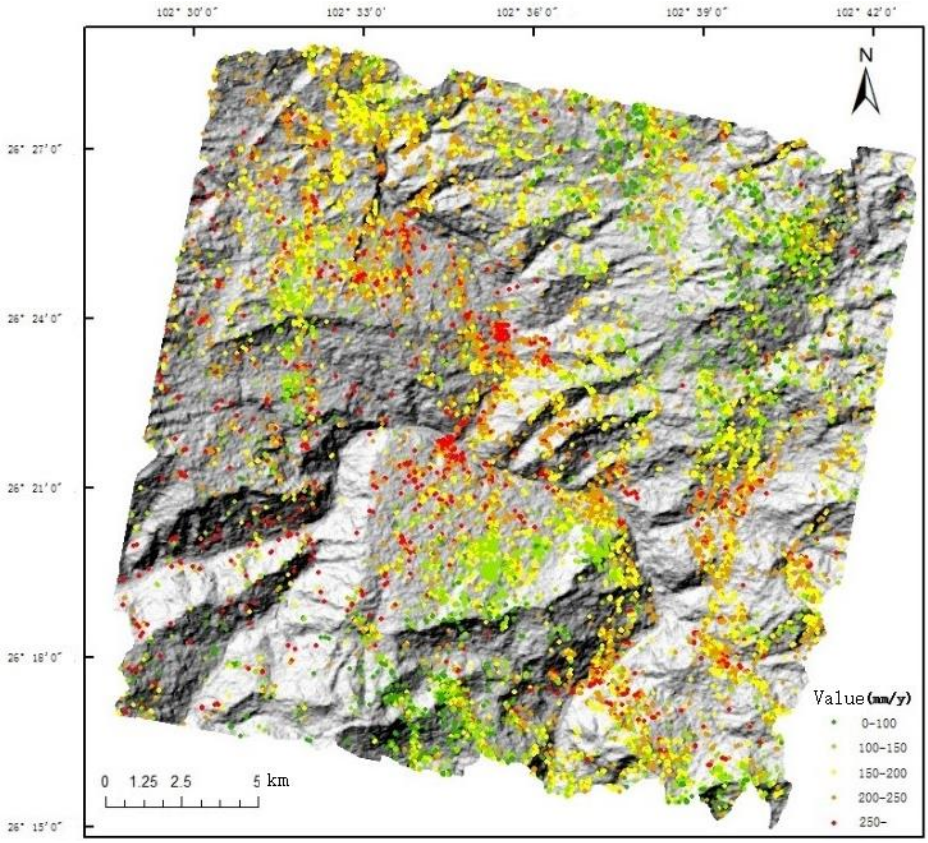

Fig. 4. PS points distribution

4. PS-INSAR MONITORING ERROR ANALYSIS

4.1. ERROR SOURCES

Although PS-InSAR technology is a drastic improvement over conventional InSAR technology, for example, in the enhancement of precision by effectively overcoming the influence of time-invariant and atmospheric interferences, many errors are still generated during the differential interference process and derived from the analysis of PS-InSAR technology based on the error characteristics of InSAR.

1) Orbit errors

The first step in the PS-InSAR technical process is baseline estimation. The ba-

sis for baseline estimation is the satellite ephemeris, also known as the orbit. Orbit errors are important parameters for calculating baseline, deformation, and DEM errors. Orbit errors are the source of baseline errors, and baseline errors lead to a failure in the formation of relative interference. Therefore, it is crucial to eliminate orbit errors. Orbit errors can only be calculated from the reference interval, the elevation error, and the error interval of the simulated interferogram based on the satellite ephemeris function. Consequently, it is not possible to directly correct orbit errors (Liao et al. 2003; He et al. 2009). Hanssen et al. proposed a polynomial correction function of orbit errors that can significantly reduced the influence of orbit errors. (Hanssen 2001). However, the error of residual short-wavelength orbits still cannot be eliminated.

2) Atmospheric errors

An atmospheric error is the delay of a signal and the bending of a propagation path due to the influence of the atmosphere during the propagation of electromagnetic waves. Atmospheric errors result in interferometric phase delay. The atmospheric effect can be removed by setting a high temporal uncorrelated threshold and a low spatial correlation threshold. However, the troposphere and ionosphere affect the propagation of a signal, and a high degree of randomness and instability exists in the magnitude and range of the signal. Therefore, in PS-InSAR technology, it is still difficult to remove atmospheric errors.

3) DEM errors

An external DEM for terrain phase removal is crucial for processing InSAR data. Due to errors in DEM data and the offset between the vertical heights of the target and the neighboring DEM, the terrain residual still exists after the terrain phase is eliminated.

This study introduced high-precision total station monitoring data, combined the advantages of the two monitoring technologies, and proposed an error elimination method based on the measured data. The errors in the PS-InSAR monitoring data due to the aforementioned factors were eliminated simultaneously, and the monitoring accuracy of PS-InSAR technology was improved considerably.

4.2. PS-INSAR ERROR CORRECTION

PS-InSAR technology can be used to monitor wide-area landslides. This technology can monitor potential landslides and dangerous deformation areas with large surface deformation and can achieve continuous monitoring over a long time series. However, single-point monitoring accuracy is not sufficient. High-precision total station monitoring technology is widely used for landslide monitoring due to the high accuracy of

single-point monitoring. In this study, the merits of these two technologies were combined to eliminate displacement errors in PS-InSAR monitoring at a single monitoring point, and the continuous surface displacement monitoring of landslides over a long period of time was obtained.

1) Monitoring point selection

Twenty-nine high-precision total station monitoring points were installed over the Jinpingzi landslide, and total station monitoring took place from 2005 to 2009. The mean displacements of all PS points in a 20-m buffer of the total station monitoring point were compared with the total station monitoring results. The distribution of the total station and PS points is displayed in Fig. 5.

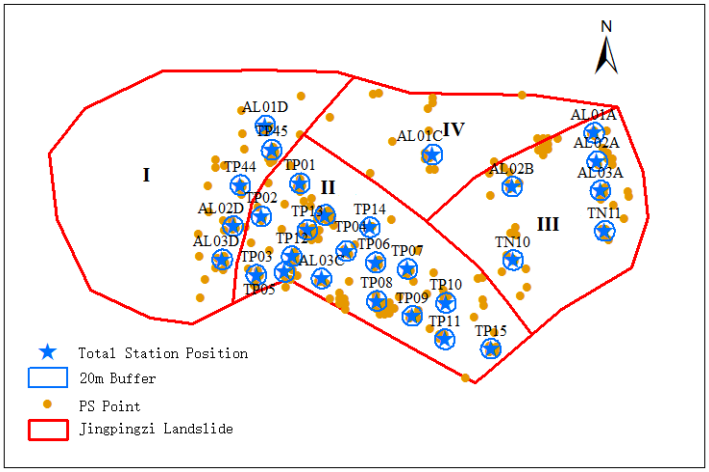

Fig. 5. Monitoring points map

The total station monitoring results revealed that the overall displacements in zones I, III, and IV were small. The total displacement during the monitoring period was approximately 20 mm, except for the total displacement of AL01D, which was 200 mm. The displacements of zone II were very obvious, and the displacements of most monitoring points were more than 1 m. PS-InSAR technology can monitor the landslide area, and the monitored overall movement trends are consistent with the actual measured trend results. Single-point monitoring results are not highly accurate; in particular, individual points always have substantial errors. By comparing and analyzing the two monitoring results, a linear fitting relationship in time series can be determined. Figure 6 illustrates the relational curves of points TP01–14.

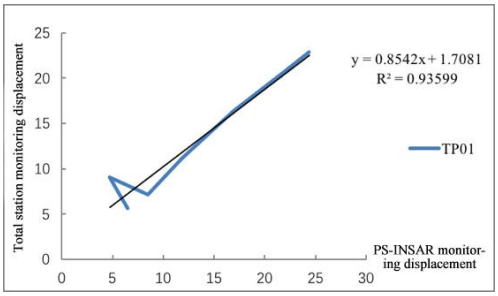
Total station monitoring displacement
y = 0.8542x + 1.7081
R² = 0.93599
TP01
PS-INSAR monitoring displacement

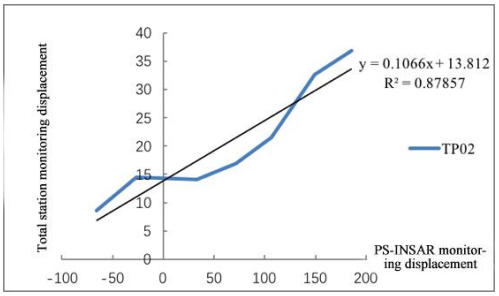
Total station monitoring displacement
y = 0.1066x + 13.812
R² = 0.87857
TP02
PS-INSAR monitoring displacement

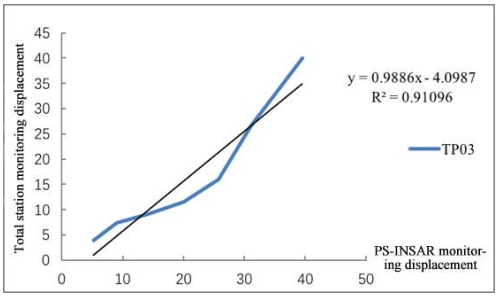
Total station monitoring displacement
y = 0.9886x - 4.0987
R² = 0.91096
TP03
PS-INSAR monitoring displacement

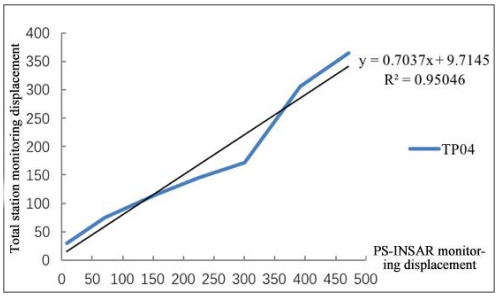
Total station monitoring displacement
y = 0.7037x + 9.7145
R² = 0.95046
TP04
PS-INSAR monitoring displacement

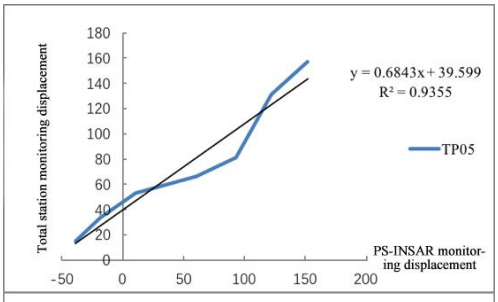
Total station monitoring displacement
y = 0.6843x + 39.599
R² = 0.9355
TP05
PS-INSAR monitoring displacement

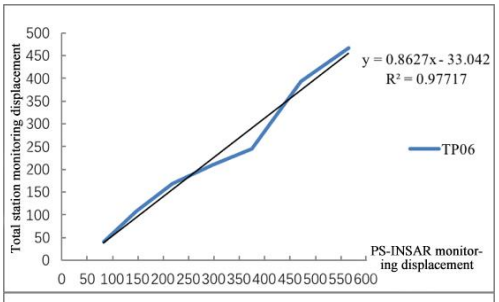
Total station monitoring displacement
y = 0.8627x - 33.042
R² = 0.97717
TP06
PS-INSAR monitoring displacement

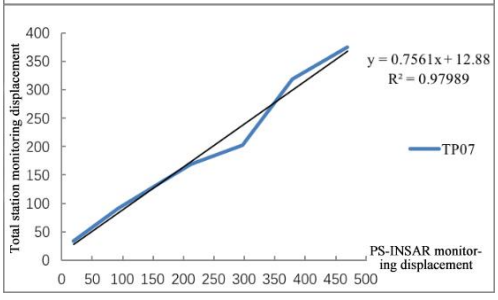
Total station monitoring displacement
y = 0.7561x + 12.88
R² = 0.97989
TP07
PS-INSAR monitoring displacement

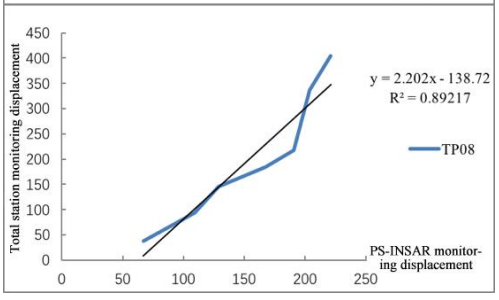
Total station monitoring displacement
y = 2.202x - 138.72
R² = 0.89217
TP08
PS-INSAR monitoring displacement

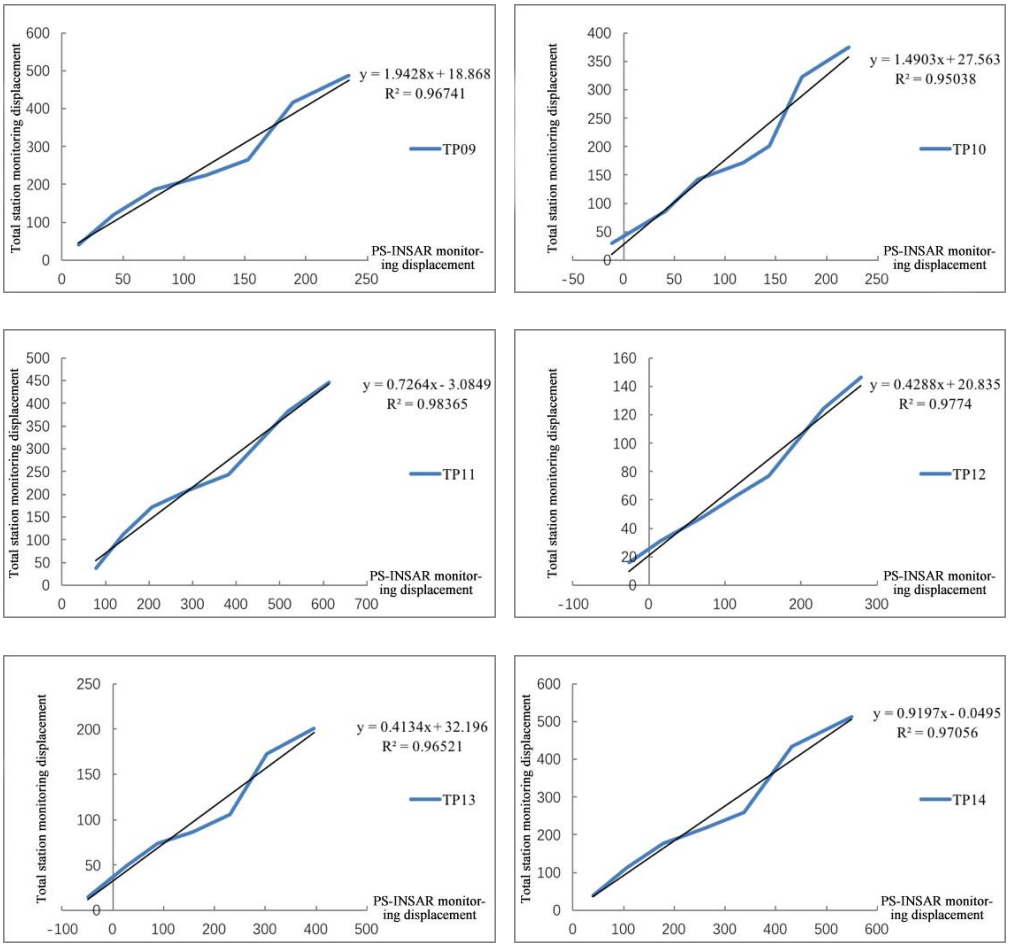

Fig. 6. Monitoring results diagram (units: mm)

2) Point displacement correction

The average value of the monitored displacement at the total station monitoring point and the PS points in the buffer satisfies the linear relationship in the time series. The notation of the fitting equation is as follows:

$$G(x_i, z_i, y_i = R_i * P(x_i, y_i, z_i) + C, \quad i = 1, 2, 3, \ldots, n. \tag{1}$$

The modified equation is:

$$P'(x_i, z_i, y_i = R_i * P(x_i, y_i, z_i), \tag{2}$$

where n is the total station monitoring point, R_i is the slope of the fitted equation, $G(x_i, y_i, z_i)$ is the displacement value of the i-th total station monitoring point, $P(x_i, y_i, z_i)$ is the average displacement value of the PS points in the i-th buffer, and $P'(x_i, y_i, z_i)$ is the corrected average displacement value of the PS points in the i-th buffer.

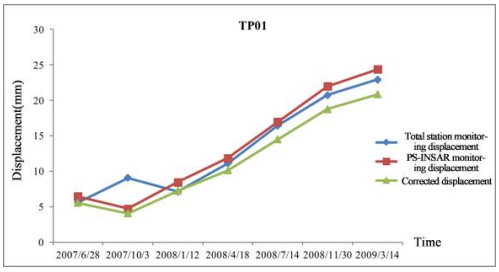

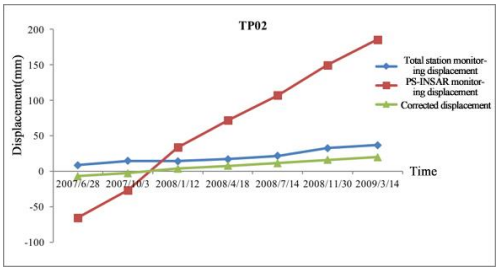

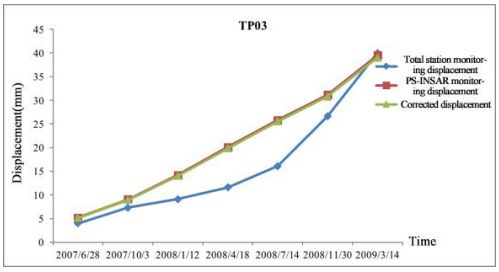

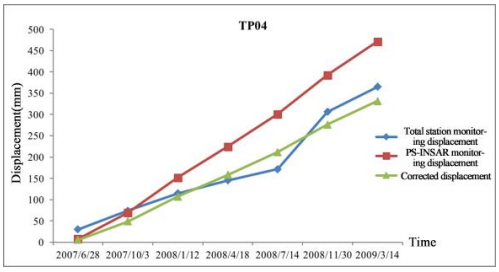

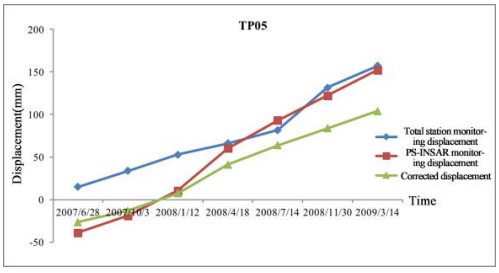

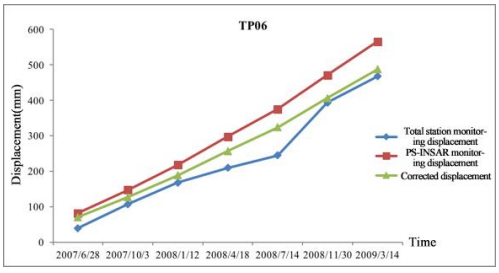

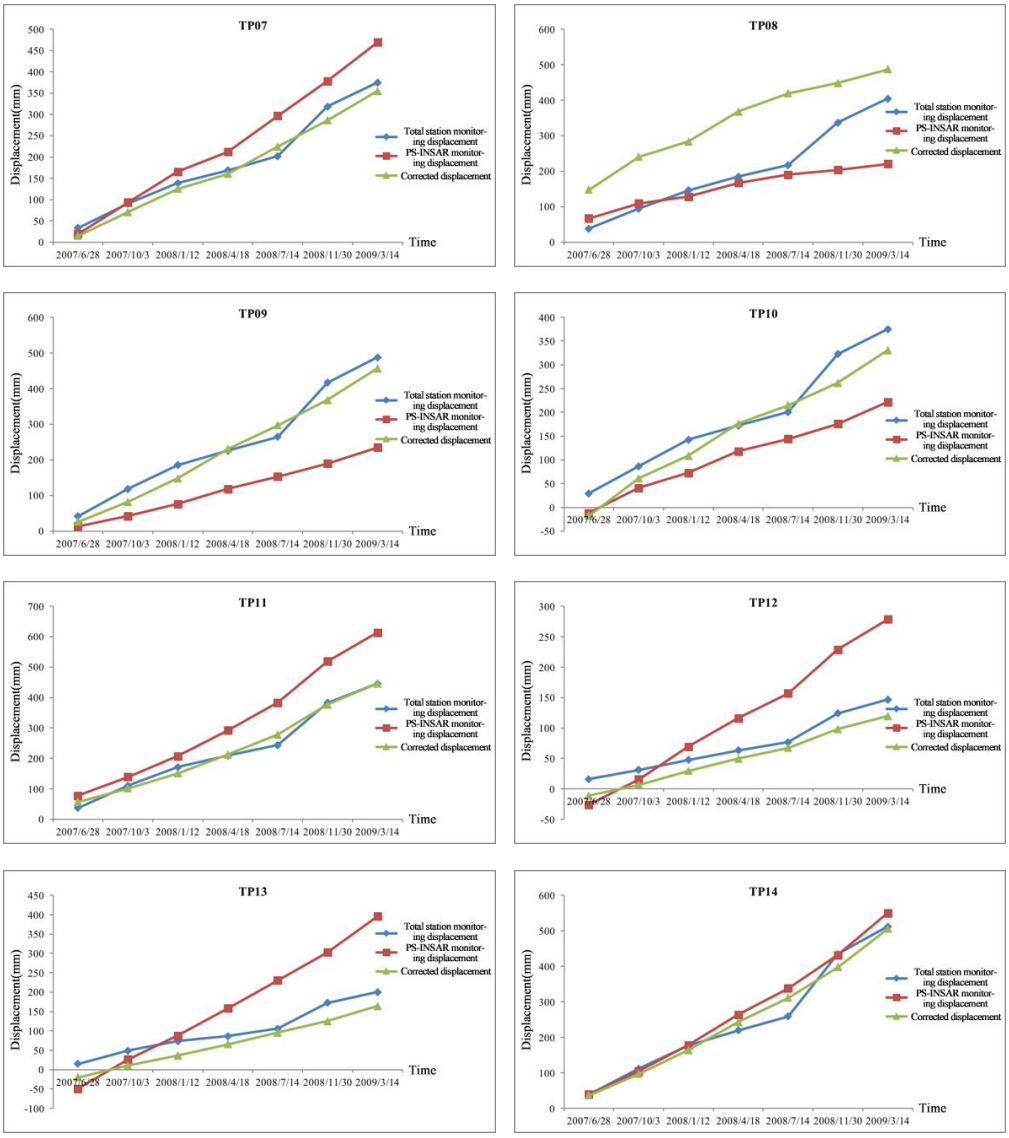

Fig. 7. Monitoring displacement and corrected displacement comparison chart

Based on the linear relationship between the total station displacement data and PS-InSAR displacement data in the time series, the deviation ratio values R_i of the monitored displacement values were obtained. The obtained deviation ratio (x_i, y_i, z_i) was substituted into formula (2) for back-calculation. After corrections were made, the PS point monitoring shift value $P'(x_i, y_i, z_i)$ was obtained. The corrected error of points TP01–14 is illustrated in Fig. 7.

From the comparison results before and after error corrections were made in the time series, as shown in Fig. 7, it was revealed that the PS-InSAR monitoring results in the smallest displacements of the Jinpingzi landslide were always larger than those of the total station. Based on this result, PS-InSAR single-point monitoring accuracy was determined. The error antialgorithm enabled the determination of the PS point displacement correction value in the buffer of the total station, which improved the PS-InSAR single-point monitoring accuracy. The corrected displacement result is in agreement with the total station result.

3) Surface displacement correction

The displacement of the landslide is a planar distribution. The correction of the displacement value of the PS points outside the buffer of the total station on the landslide can more accurately reflect changes in the surface displacement of the landslide. The Kriging method was introduced into the error correction model, and the deviation ratio was used as the interpolation criterion of this model to obtain the deviation ratio of all PS points in the landslide area. Based on the error fusion algorithm presented in Equation 2, the correction displacement values of all PS points in the landslide area were calculated and the landslide surface displacement distribution map was obtained.

Kriging interpolation is a spatial interpolation method based on mathematical and statistical models. After the point data were obtained, the Kriging model was used to calculate the distribution of the obtained data on the surface, which is an effective grid geostatistical method. This method provides an optimal linear unbiased estimation method by using known sample point attribute values in the region, thus assigning a certain coefficient to each sample point and finally estimating the attribute values of other interpolation points in the region by using a weighted average (Niu et al. 2001; Li et al. 2013). When the number of data points is large, the credibility of the interpolation results is higher. The hypothesis model is as follows:

$$R(x_0) = \sum_{i=1}^{n} \gamma_i R(x_i). \tag{3}$$

In the formula, x_0 is the PS point to be interpolated, $R^*(x_0)$ is the deviation ratio of the PS point to be interpolated, and γ_i is the weight of the variable $R(x_i)$. The variogram model is used to find γ_i:

$$\mathrm{Var}[R(x_i) - R(x_j)] = 2\mu(x_i, x_j) = 2\mu(c), \tag{4}$$

where $c = x_i - x_j$, which is the distance between point x_i and point x_j. To minimize γ_i, the distance between the point to be interpolated and the known point can be used to obtain the weight $\gamma_{i\,\min}$. Let $V[R^*(x_0) - R(x_0)] = \gamma_{i\,\min}$. Then, the Lagrangian multiplier was to construct the function and find the weight γ_i. By substituting γ_i into Eq. (3), the deviation ratio $R^*(x_0)$ of the PS point to be interpolated was finally obtained.

After the deviation ratio $R^*(x_0)$ of all the PS points to be interpolated in the landslide region was derived, the PS-InSAR monitoring displacement value $P(x_i, y_i, z_i)$ was substituted into Eq. (2). Next, the corrected displacement value $P'(x_i, y_i, z_i)$ of all the PS points to be interpolated was calculated to realize the error correction of all PS points in the landslide and finally to obtain the monitoring result of the landslide surface displacement.

4.3. FIELD APPLICATION

1) Total station surface displacement distribution

In this study, the monitoring data of the shooting time from the master images of 6, 12, 20 months were selected. The surface displacement distribution maps of the 29 total station monitoring points were obtained using the Kriging difference method, as shown in Fig. 8. The displacement map of the landslide surface can more clearly present the actual movement of the landslide. The figure reveals that the displacement in zone II is the most obvious.

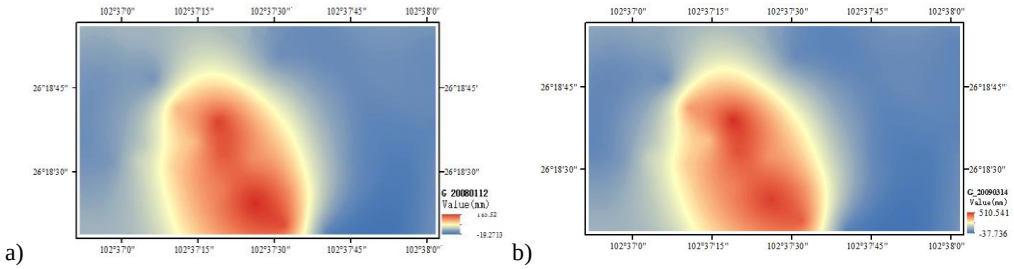

Fig. 8. Total station monitoring of surface displacement distribution

2) Corrected PS-InSAR surface displacement distribution

Figure 9 presents the PS-InSAR surface displacement map after error corrections were conducted. The figure presents the distribution of the surface displacements over different time series.

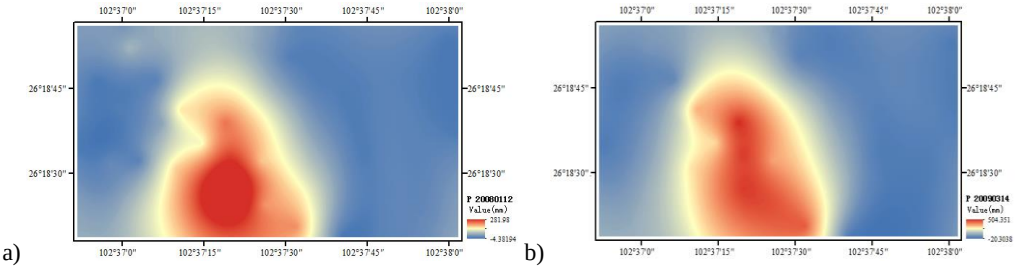

Fig. 9. Correct PS-InSAR surface displacement map

3) Data comparison

By comparing the surface displacement maps obtained by the two monitoring techniques, it was revealed that the displacement deformation trends are similar, but some errors were still present. The aforementioned surface displacement map was subjected to differential calculation to simultaneously obtain the difference of each grid unit. Then, the surface displacement error values of the two monitoring technologies were obtained, as shown in Fig. 10. The error values between the two surface monitoring methods in each time series were within 2 cm. Therefore, it that the error correction method based on the total station monitoring results can improve the monitoring accuracy of PS-InSAR technology.

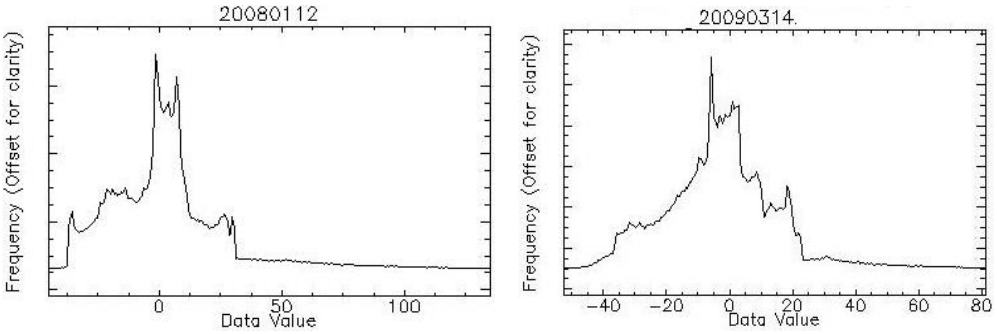

Fig. 10. Monitoring result error chart

4) Modified PS-InSAR to monitor landslide displacement

The PS-InSAR monitoring data for the Jinpingzi landslide from January 2007 to March 2009 were corrected for displacement, as presented in Fig. 11. Before errors are

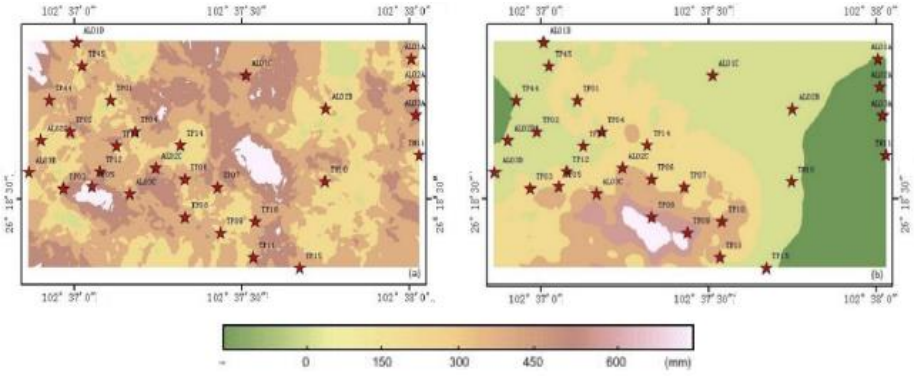

Fig. 11. Corrected before and after displacement comparison chart

eliminated, PS-InSAR monitoring results can reveal the overall changes in the landslide, but the displacement map is scattered. After errors were removed, the trend and results of the displacement within the study area were basically consistent with the on-site monitoring results that was provided by the Three Gorges Hospital. After corrections were made, the displacement values of the landslide coincided well with the actual displacement values of the landslide. This result reveals that the proposed method is feasible and realizes the monitoring of the surface displacement of the peristaltic landslide in a long time sequence. Moreover, the surface displacement map can show the sliding state of the landslide better and more clearly than the single-point monitoring results can, thus providing a more intuitive method for the prevention and control of landslide hazards.

5. DISCUSSION

To allow for better application of PS-InSAR technology for monitoring the deformation of slow-moving landslides, this study selected the Jinpingzi landslide located in the Wudongde Reservoir area as the area under study and verified the practicality of the PS-InSAR technique for monitoring slow-moving landslides by placing total station monitoring points on the landslide.

The monitoring data acquired using the PS-InSAR technology and the total station were consistent in the studied time series, and a linear relationship was observed between them. The fitting equation was obtained by comparing the distribution characteristics of the displacement value of the total station monitoring point and the PS point average displacement value in the 20 m buffer zone. The slope of the fitting equation is the ratio of the deviation between the two monitoring errors. Thus, the corrected PS point monitoring displacement value can be inversely calculated using this ratio.

To fully utilize the advantages of PS-InSAR technology for monitoring landslide surface deformation and for conducting high-precision single-point monitoring of total stations, the deviation ratio of these two monitoring methods was used as the basis for interpolation. The Kriging interpolation method was used to derive the ratio of other PS points to be interpolated in the landslide area. Through the error antialgorithm, the corrected displacement values of the PS points in the entire landslide area were obtained, thereby enabling the monitoring of a slow-moving landslide over a long time sequence.

By comparing the two types of monitoring results of the surface displacement map, it was revealed that the planar distribution results of the two monitoring techniques were consistent in the time series. The difference between the surface displacement values of the same time series was calculated, and the statistical results of the surface displacement difference were derived. The error values of the two monitoring techniques obtained were small, and the reliability of the correction

results was proved.

6. CONCLUSION

By using the Jinpingzi landslide as an example, the feasibility of the PS-InSAR error analysis method based on the total station monitoring results was verified. This correction method can eliminate the monitoring error in PS-InSAR technology and overcome the limitations of PS-InSAR single-point monitoring accuracy. Moreover, the proposed method can compensate for the limitation that the high-precision total station cannot analyze the sliding surface displacement of the landslide as a whole. This method is especially suitable for zones that must be monitored over a wide area. First, PS-InSAR technology can be used to monitor large areas. Then, high-precision total stations or other high-precision instruments can be installed in key places with large deformations to eliminate PS-InSAR single-point monitoring errors and improve landslide surface displacement determination. All these factors benefit observation accuracy and enable the high-precision monitoring of the surface displacement of a peristaltic landslide in a long time series.

REFERENCES

LIAO M.S., LIN H., 2003, *Radar Interferometry: Principles and Signal Processing Basics*, Surveying and Mapping Press, Beijing, China.

HANSSEN R.F., 2001, *Radar interferometry: data interpretation and error analysis*, Springer Science & Business Media, Berlin, Germany.

BIANCHINI S., CIGNA F., RIGHINI G. et al., 2012, *Landslide HotSpot Mapping by means of Persistent Scatterer Interferometry [J]*, Environmental Earth Sciences, Vol. 67, No. 4, 1155–1172, DOI: 10.1007/s12665-012-1559-5.

BIANCHINI S., HERRERA G., MATEOS R.M., et al., 2013, *Landslide Activity Maps Generation by Means of Persistent Scatterer Interferometry [J]*, Remote Sensing, Vol. 5, No. 12, 6198–6222. DOI: 10.3390/rs5126198.

BOVENGA F., NUTRICATO R., REFICE A. et al., 2006, *Application of multi-temporal differential interferometry to slope instability detection in urban/peri-urban areas [J]*, Engineering Geology, Vol. 88, No. 3, 218–239, DOI: 10.1016/j.enggeo.2006.09.015.

CALVELLO M., PEDUTO D., ARENA L., 2016, *Combined use of statistical and D-InSAR data analyses to define the state of activity of slow-moving landslides [J]*, Landslides, Vol. 14, No. 2, 1–17, DOI: 10.1007/s10346-016-0722-6.

CATANI F., FARINA P., MORETTI S. et al., 2005, *On the application of SAR interferometry to geomorphological studies: estimation of landform attributes and mass movements [J]*, Geomorphology, Vol. 66, No. 1–4, 119–131, DOI: 10.1016/j.geomorph.2004.08.012.

CRUDEN D.M., 1996, *Landslides Types and Processes[J]*, *Landslides. Investigation and Mitigation*, 36–75.

FERRETTI A., PRATI C., ROCCA F., 2001, *Permanent scatterers in SAR interferometry [J]*, IEEE Transactions on Geoscience & Remote Sensing, Vol. 39, No. 1, 8–20, DOI: 10.1109/36.898661.

FERRETTI A., PRATI C., ROCCA F., 2000, *Analysis of permanent scatterers in SAR interferometry [C]*, Geoscience and Remote Sensing Symposium, 2000. Proceedings. IGARSS 2000. IEEE 2000 International, IEEE, No. 2, 761–763, DOI: 10.1109/IGARSS.2000.861695.

HASTAOGLU K.O., 2016, *Comparing the results of PSInSAR and GNSS on slow motion landslides, Koyulhisar, Turkey [J]*, Geomatics Natural Hazards & Risk, Vol. 7, No. 2, 786–803, DOI: 10.1080/19475705.2014.978822.

HE P., XU C.J., 2009, *Research on effects of satellite orbit error on SAR interferometry [J]*, Journal of Geodesy and Geodynamics, Vol. 29, No. 5, 54–57, DOI: 10.3969/j.issn.1671-5942.2009.05.012 (in Chinese).

KONG J.M., 2004, *The stage feature of landslide growth and observation [J]*, Journal of Mountain Science, No. 6, 725–729, DOI: 10.3969/j.issn.1008-2786.2004.06.015 (in Chinese).

LEI L., ZHOU Y., LI J. et al., 2012, *Application of PS-InSAR to monitoring Berkeley landslides [J]*, Journal of Beijing University of Aeronautics and Astronautics, Vol. 38, No. 9, 1224–1226, DOI : 10.13700/j.bh.1001-5965.2012.09.005.

LI J.X., LI C.K., YIN Z.H., 2013, *ArcGIS based kriging interpolation method and its application [J]*, Bulletin of Surveying and Mapping, No. 9, 87–90 (in Chinese).

LU P., CATANI F., TOFANI V. et al., 2014, *Quantitative hazard and risk assessment for slow-moving landslides from Persistent Scatterer Interferometry [J]*, Landslides, Vol. 11, No. 4, 685–696, DOI: 10.1007/s10346-013-0432-2.

NIU W.J., ZHU D.P., CHEN Q.M., 2001, *Improvement of Moving Neighborhood Kriging Method [J]*, Journal of Computer Aided Design and Computer Graphics, Vol. 13, No. 8, 752–756, DOI: 10.3321/j.issn:1003-9775.2001.08.015 (in Chinese).

SINGHROY V., ALASSET P.J., COUTURE R. et al., 2007, *InSAR monitoring of landslides on permafrost terrain in Canada [C]*, Geoscience and Remote Sensing Symposium, 2007, IGARSS 2007, IEEE International, 2451–2454, DOI: 10.1109/IGARSS.2007.4423338.

WANG G.J., XIE M.W., CHAI X.Q., et al., 2013, *D-InSAR-based landslide location and monitoring at Wudongde hydropower reservoir in China [J]*, *Environmental Earth Sciences*, Vol. 69, No. 8, 2763–2777, DOI: 10.1007/s12665-012-2097-x.

WANG G.J., XIE M.W., QIU C. et al., 2011, *Experiment research of D-InSAR technique on identifying landslide moving in a wide area [J]*, Journal of University of Science & Technology Beijing, Vol. 33, No. 2, 131–141, DOI: 10.13374/j. issn1001-053x.2011.02.021 (in Chinese).

XIE M.W., HUANG J.X., WANG L.W. et al., 2016, *Early landslide detection based on D-InSAR technique at the Wudongde hydropower reservoir [J]*, Environmental Earth Sciences, Vol. 75, No. 8, 1–13, DOI: 10.1007/s12665-016-5446-3.

XU Q., 2012, *Theoretical studies on prediction of landslides using slope deformation process data [J]*, Chinese Journal of Engineering Geology, Vol. 20, No. 2, 145–151, DOI: 10.3969/j.issn.1004-9665.2012.02.001 (in Chinese).